catalysts

MDPI

Article

Catalytic Behaviors of Supported Cu, Ni, and Co Phosphide Catalysts for Deoxygenation of Oleic Acid

Nopparuj Kochaputi [1], Chanapa Kongmark [1,2,*], Pongtanawat Khemthong [2,3,*], Teera Butburee [2,3], Sanchai Kuboon [2,3], Attera Worayingyong [1] and Kajornsak Faungnawakij [2,3]

1 Department of Materials Science, Faculty of Science, Kasetsart University, Bangkok 10900, Thailand
2 Research Network of NANOTEC—KU on NanoCatalysts and NanoMaterials for Sustainable Energy and Environment, Kasetsart University, Bangkok 10900, Thailand
3 National Nanotechnology Center (NANOTEC), National Science and Technology Development Agency (NSTDA), Pathumthani 10900, Thailand
* Correspondence: chanapa.k@ku.th (C.K.); pongtanawat@nanotec.or.th (P.K.); Tel.: +66-2562-5555 (ext. 646521) (C.K.); +66-2117-6612 (P.K.)

Received: 27 July 2019; Accepted: 20 August 2019; Published: 24 August 2019

Abstract: Catalytic behaviors of copper phosphide supported on various oxides (SiO_2, γ-Al_2O_3, and USY zeolite) have been evaluated for deoxygenation of oleic acid and compared with nickel and cobalt phosphides. All catalysts were prepared by the hydrogen reduction of metal phosphate precursors. CoP and Ni_2P were obtained on USY zeolite, while Cu_3P was formed on USY and SiO_2 supports. On the contrary, the metallic Cu phase was stabilized on γ-Al_2O_3 support. Metal phosphide particles were highly dispersed on the USY support. Cu_3P/USY exhibited much larger surface area and higher acidity compared to Cu_3P/SiO_2, owing to the textural and acidic properties of the USY zeolite support. All supported catalysts gave an oleic acid conversion close to 100% at 340 °C. Ni_2P/USY, CoP/USY, and Cu/γ-Al_2O_3 favored the deoxygenation of oleic acid to alkane products such as heptadecane and octadecane. Highly selective production of octadecane (98%) through hydrodeoxygenation pathway occurred on Cu/γ-Al_2O_3. In contrast, the supported Cu_3P catalysts favored cyclization and aromatization to form cyclic and aromatic compounds such as dodecylcyclohexane, heptylcyclopentane, and dodecylbenzene. Cu_3P/SiO_2 provided dodecylbenzene in higher yield (46%) than Cu_3P/USY (33%).

Keywords: deoxygenation; oleic acid; copper; copper phosphide; nickel phosphide; cobalt phosphide

1. Introduction

As oil reserves have become exhausted and the rate of fossil fuel consumption for energy continues to increase, a renewable biofuel such as the biodiesel, aliphatic ester, vegetable oil, and biomass-derived fatty acid has been receiving considerable attention due to economic, environmental, and social benefits [1–3]. However, renewable biofuels contain a significant amount of unsaturated bonds and oxygenated functional groups, resulting in undesirable properties, such as low energy density, high acidity, poor chemical stability, and high viscosity. Therefore, upgrading the renewable biofuel by removing the oxygen atoms and producing linear hydrocarbons, also known as bio-hydrogenated diesel (BHD) or green diesel, is required before using as a drop-in replacement for traditional petroleum fuels.

The deoxygenation reaction, including hydrodeoxygenation (HDO), decarbonylation (DCO), and decarboxylation (DCO_2), is one of the most important upgrading processes of renewable biofuel [4–6], which utilizes hydrogen in the presence of a catalyst to selectively remove oxygen present in renewable biofuel. Extensive research has been performed on various catalysts, for example, transition metals [7–11], metal sulfides [6,7,12], metal oxides [7,13], metal borides [14,15], metal carbides [16], metal nitrides [17,18], and metal phosphides [19–24]. Among these catalysts, metal phosphides show excellent catalytic properties and high stability to remove oxygen from bio-oil compounds. Cecilia and coworkers [23] have investigated the catalytic performance of Ni_2P catalysts for HDO at moderate temperature (300 °C) by using dibenzofuran as a model compound and found that phosphides could prevent deactivation of a catalyst from water and coke formation on the catalyst. Interestingly, these catalysts exhibited high selectivity for the hydrogenation pathway. Various metal phosphides on silica such as Ni_2P/SiO_2, Fe_2P/SiO_2, MoP/SiO_2, Co_2P/SiO_2, and WP/SiO_2 have been tested for HDO of guaiacol (a main product from fast pyrolysis biomass) in gas phase [19,24]; benzene and phenol were obtained as main products. The addition of Cu strongly affected the acidity of the NiCu catalyst [25], achieving the cyclohexane selectivity of 80.8% and the methylcyclohexane selectivity of 12.4%. Soták and coworkers have also reported the potential use of carbon-supported Cu_3P catalyst for hydrogenolysis of polyalcohols derived from biomass, that is, glucose, sorbitol, and xylitol, to ethylene and propylene glycols [26]. Therefore, it is expected that the application of copper phosphide catalyst would enhance the catalytic activity in bio-oil HDO reactions. To the best of our knowledge, there have been no studies on the catalytic performance of copper phosphide for deoxygenation of renewable biofuel.

In addition, it is known that the nature of support materials can affect the structure, purity, morphology, surface area, and acidity of catalysts, which exert significant influence on their catalytic properties [19,27]. Shi and coworkers have illustrated the effect of support on structure and catalytic activity properties of metal phosphides [27]. They found that nickel phosphide species could adopt various crystal structures depending on types of support material. For example, Ni_2P phase was formed on SiO_2, CeO_2, TiO_2, and SAPO-11, while Ni_3P and $Ni_{12}P_5$ phases were stabilized on γ-Al_2O_3. On the other hand, the mixed phases of $Ni_{12}P_5$ and Ni_2P species were observed on HY zeolite. These different forms of nickel phosphide catalyst on various supports also play an important role in the catalytic performance for the deoxygenation of methyl laurate to C_{11} and C_{12} hydrocarbons. Therefore, the effect of support materials on various metal phosphide catalysts should be thoroughly investigated in order to understand the nature of catalysts and their catalytic performance.

In the present work, deoxygenation of oleic acid has been evaluated over a series of copper phosphide supported on various oxides (SiO_2, γ-Al_2O_3, and USY zeolite) and compared with nickel and cobalt phosphides supported on USY zeolite. All catalysts were prepared by the hydrogen reduction of impregnated metal phosphate precursors and characterized by X-ray diffraction (XRD), scanning electron microscopy (SEM), nitrogen adsorption–desorption isotherms, and temperature-programmed desorption of ammonia (NH_3-TPD). Catalytic behaviors of catalysts were evaluated for deoxygenation of oleic acid at 260–340 °C and 50 bar. Oleic acid was employed as a model compound to gain insight into the deoxygenation reaction of fatty acids, an essential step to convert renewable biofuel into fuels and value-added chemicals. The evolution of oleic acid conversion and product yields have been studied as a function of reaction temperature. The effect of catalyst compositions and support materials on the structure, surface property, activity, and selectivity of catalysts have been explored.

2. Results and Discussion

2.1. Crystal Structures

Crystal structures of supported catalysts were investigated by means of X-ray diffraction (XRD). XRD patterns of all catalysts are presented in Figure 1. Apart from the diffraction peaks due to supports, Cu_3P characteristic peaks at 2θ = 36.0°, 39.1°, 41.6°, 45.1°, 46.2°, and 47.3° (PDF no. 01-071-2261) were observed for Cu_3P/SiO_2 and Cu_3P/USY catalysts. Single-phase Cu_3P particles were successfully obtained on SiO_2 and USY supports, whereas metallic Cu phase (PDF no. 01-089-2838) was stabilized on γ-Al_2O_3 support. Shi and coworkers have reported that metal phosphide catalyst could adopt several structures depending on support materials [27]. For Ni_2P/USY, the formation of Ni_2P was confirmed by signature peaks at 2θ = 40.7°, 44.5°, 47.3°, 54.1°, and 55.0° (PDF 01-089-2742) and no evidence of impurities was observed. CoP/USY displayed characteristic peaks of CoP (2θ = 31.6°, 46.2°, 48.1°, 56.0°, and 56.8°, PDF 03-065-1474) which has been reported to exhibit higher activity and stability than Co_2P in the hydrotreating processes [28]. A peak of cristobalite SiO_2 was also noticed (21.6°) in the diffraction pattern of CoP/USY, which could result from the partial decomposition of USY zeolite at high temperature [29] as the reduction temperature of CoP/USY (750 °C) was higher than other supported metal phosphides (650 °C). The average crystallite size of metal and metal phosphide catalysts, estimated from the XRD peak width by using the Debye Scherrer equation, varied in the range of 33–60 nm (Table 1). Cu_3P/USY and Cu_3P/SiO_2 had the smallest crystallite size, followed by Ni_2P/USY, Cu/γ-Al_2O_3, and CoP/USY.

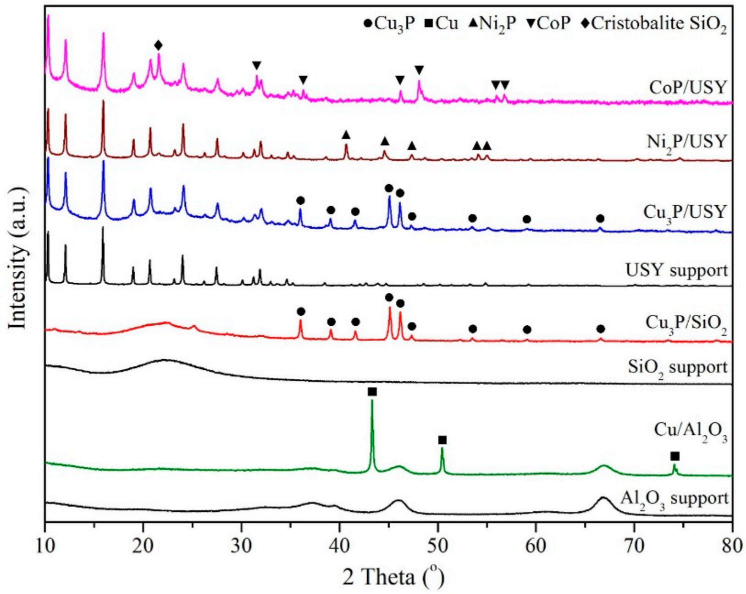

Figure 1. XRD patterns of supported metal and metal phosphide catalysts.

Table 1. Surface properties of catalysts and supports.

Catalyst	Acid Site (mmol/g) [a]	S_{BET} (m^2/g)	S_{micro} (m^2/g)	Total Pore Volume (cc/g)	Micropore Volume (cc/g)	Pore Diameter (nm)	Crystallite Size (nm) [b]
CoP/USY	0.19	247	95	0.28	0.06	3.7	58.4
Ni_2P/USY	0.60	446	321	0.24	0.17	3.7	39.2
Cu_3P/USY	0.34	371	253	0.24	0.13	3.7	33.2
Cu_3P/SiO_2	0.04	38	-	0.50	-	27.2	33.2
Cu/γ-Al_2O_3	0.50	101	-	0.31	-	7.8	46.0
USY	0.52	696	558	0.27	0.26	3.7	-
SiO_2	-	471	-	0.99	-	6.9	-
γ-Al_2O_3	0.43	198	-	0.54	-	7.8	-

[a] Determined from NH_3-TPD; [b] Determined from XRD.

2.2. *Morphology and Surface Properties*

The morphologies of supported copper and metal phosphide catalysts are illustrated in Figure 2. SEM micrographs, recorded with a backscattering mode (BSE), show specimen contrast due to the variation of atomic weights. In general, the brighter areas were Cu, Cu_3P, Ni_2P, and CoP particles deposited on each support. Small particles of Cu_3P, Ni_2P, and CoP were well dispersed on USY support, while Cu_3P particles on SiO_2 formed agglomerates of diameters ranging from 300 nm to 1.2 μm. It seems likely that the morphology and the large surface area of USY zeolite favored the dispersion of metal phosphide particles, thus shifting the average particle size of catalysts toward smaller values. For Cu/γ-Al_2O_3, Cu particles tended to agglomerate on γ-Al_2O_3 support, and different sizes of Cu metal clusters (~100 to 800 nm) were formed.

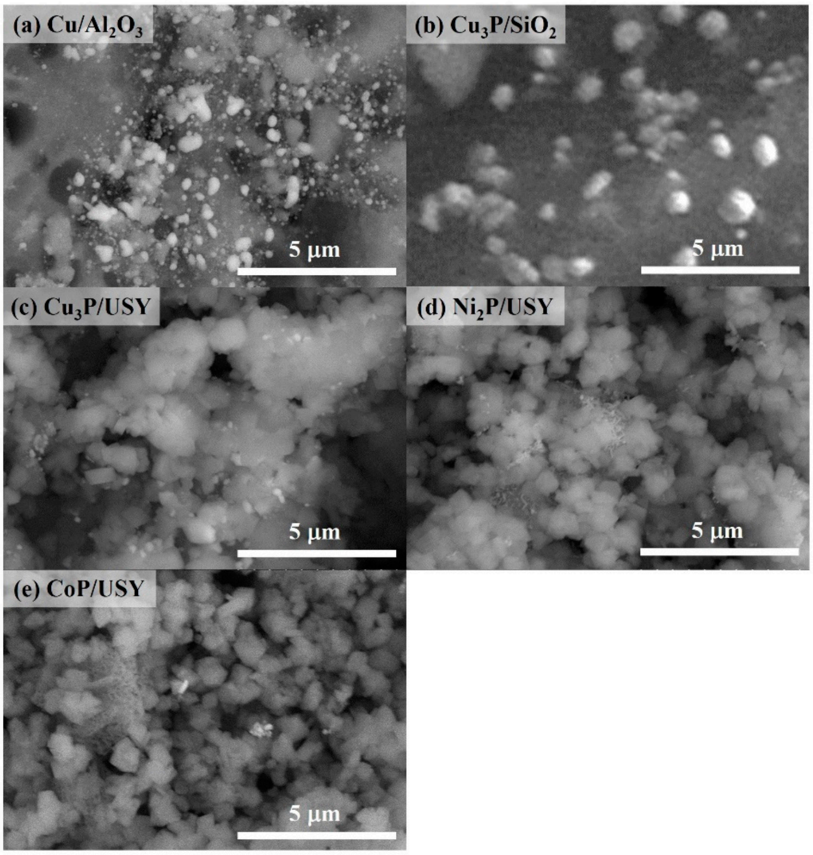

Figure 2. SEM images of supported metal and metal phosphide catalysts: Cu/γ-Al_2O_3 (**a**), Cu_3P/SiO_2 (**b**), Cu_3P/USY (**c**), Ni_2P/USY (**d**), CoP/USY (**e**).

N_2 adsorption–desorption isotherms and Barrett, Joyner, and Halenda (BJH) pore-size distributions of supported metal and metal phosphide catalysts are presented in Figures 3 and 4, respectively. The characteristic textural properties of the catalysts are summarized in Table 1.

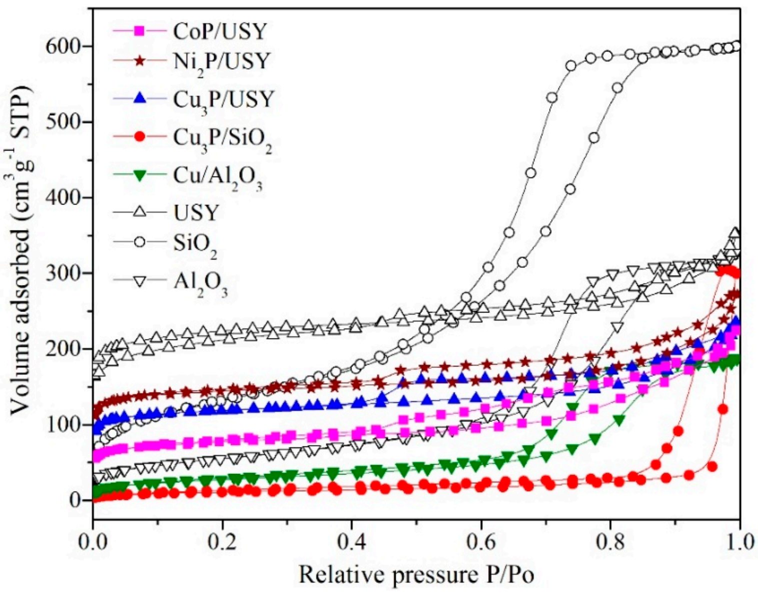

Figure 3. N_2 adsorption–desorption isotherm of supported metal and metal phosphide catalysts.

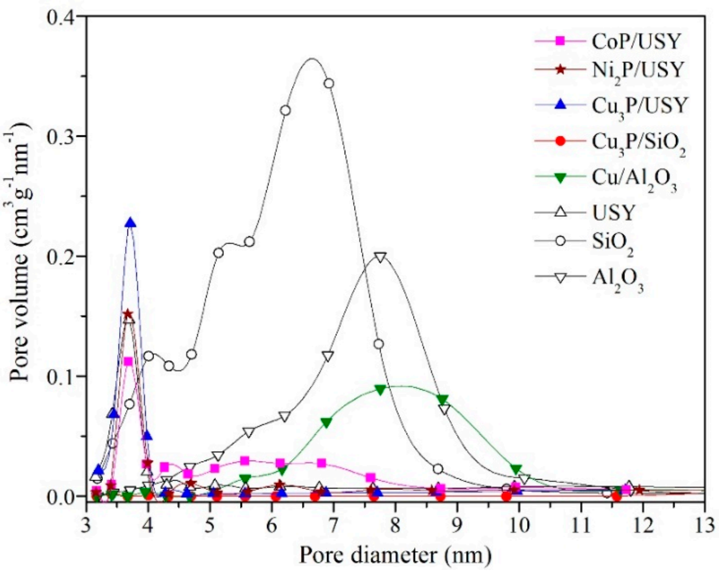

Figure 4. Pore-size distribution of supported metal and metal phosphide catalysts.

All catalysts and supports exhibited type IV isotherms (Figure 3), with hysteresis loops attributing to capillary condensation in mesopores, which are typically observed for mesoporous materials. One can also notice that the isotherms of USY support, Cu_3P/USY, N_2P/USY, and CoP/USY catalysts, rose steeply at low relative pressure ($P/P_0 > 0.1$), indicating the presence of micropores in the samples. USY is known to contain both micropores inherited from the zeolite structure and mesopores gained from the dealumination process which endow them with large surface area [30]. The USY zeolite support used in this study had the largest surface area when compared to SiO_2 and γ-Al_2O_3 supports (Table 1). In general, the textural properties of the catalysts are strongly related to the properties of the corresponding supports. Each group of catalysts on the same support displayed the same type of hysteresis loop. The USY-supported catalysts exhibited type H4 hysteresis loop characteristic of narrow slit pores, while the hysteresis loops of catalysts on other supports were of type H2, which are often associated with the ink-bottle-neck-type pores. In Figure 4, the formation of Cu_3P, N_2P, and CoP and metallic Cu particles did not significantly alter the pore character of USY (3.2–4.0, median 3.7 nm) and γ-Al_2O_3 (3.7–11.7, median 7.8 nm) supports. In contrast, Cu_3P/SiO_2 showed a dramatic decrease of surface area and pore volume. The pore character of SiO_2 (3.2–9.8, median 6.9 nm) was also suppressed after the deposition of Cu_3P catalyst on SiO_2 support. A plausible explanation for this observation is that the Cu_3P catalyst particles could fill the pores of SiO_2 support or completely block a great number of them. According to the textural properties shown in Table 1, the specific surface area followed the sequence of Ni_2P/USY > Cu_3P/USY > CoP/USY > Cu/γ-Al_2O_3 > Cu_3P/SiO_2. This difference in surface area could be influenced by the nature of the support material, the dispersion, and the crystallite size of catalysts. Therefore, a high dispersion of small Ni_2P nanoparticles on USY support would be responsible for such a large surface area of Ni_2P/USY catalyst.

The acidic properties of catalysts and supports were studied by temperature-programmed desorption of ammonia (NH_3-TPD). The NH_3-TPD profiles and concentrations of acid sites are presented in Figure 5 and Table 1, respectively. The number of acid sites in supports decreased in the following order: USY > γ-Al_2O_3 > SiO_2, and the number of acid sites in catalysts was in the order of Ni_2P/USY > Cu/γ-Al_2O_3 > Cu_3P/USY > CoP/USY > Cu_3P/SiO_2. The strength of acid site can be distinguished by the desorption temperature of the adsorbed NH_3 (T). The low-temperature desorption ($T < 250$ °C) is related to the weak acid sites, while the high-temperature desorption ($T > 250$ °C) is related to the strong acid sites [23]. USY support gave two desorption peaks at about 166 °C and 325 °C corresponding to the weak adsorption of ammonia molecules on Si–OH groups and the Brönsted acid sites, that is, bridged Si–OH–Al hydroxyl groups in Y-type zeolites, respectively [31]. The weak and strong acid sites were also observed for Cu_3P/USY, Ni_2P/USY, and CoP/USY catalysts, however, these catalysts displayed a greater amount of weak acid sites and a smaller amount of strong acid sites when compared to the pure USY support. It is possible that the deposition of metal phosphide particles could cover both weak and strong acid sites of USY support, while the metal phosphide could itself contribute Lewis and Brönsted acidity. Metal phosphides were reported to have both Brönsted (~200 °C) and Lewis (~320 °C) acid sites, which are related to the P–OH group and the electron-deficient metal site, respectively [27,32]. Therefore, the highest acidity of Ni_2P/USY could be attributed to the acidity properties of metal phosphide and USY support, the large surface area, and high dispersion of small Ni_2P particles so that NH_3 molecules could be adsorbed more readily than other catalysts. Regarding the TPD profile of Al_2O_3 support, a small broad envelope of unresolved peaks extended to 487 °C was observed, indicating the presence of strong acid sites which are related to Al Lewis acid centers (i.e., the electron acceptor sites formed by the coordinatively unsaturated aluminum ions) [33]. However, Cu/γ-Al_2O_3 exhibited a larger desorption peak at low temperature when compared to γ-Al_2O_3 support. The metallic Cu is known to possess the Lewis acidity, whereas the Brönsted acid sites could be generated from phosphate species, possibly an amorphous form that was not detectable by XRD, remaining as a consequence of their incomplete reduction [23]. Cu_3P/SiO_2 contained the least amount of acid sites, which could be related to the small surface area and the weak acidity of SiO_2 support.

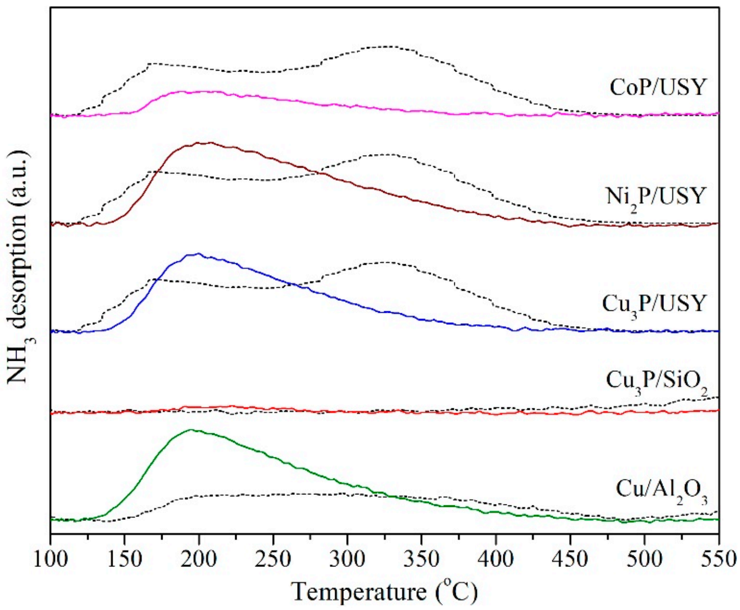

Figure 5. NH_3-TPD of catalysts and supports. Solid lines correspond to metal and metal phosphide catalysts, dash lines correspond to pure supports.

2.3. Deoxygenation of Oleic Acid

The oleic acid conversion and product yields of CoP/USY, Ni_2P/USY, Cu_3P/USY, Cu_3P/SiO_2, Cu/γ-Al_2O_3 were plotted as a function of reaction temperature, as illustrated in Figure 6, taking into account that a complete conversion was achieved over all catalysts after reaching 340 °C for 4 h. It is observed that CoP/USY (Figure 6a) and Ni_2P/USY (Figure 6b) catalysts exhibited similar catalytic behavior. At 4 h, these catalysts favored the production of heptadecane and octadecane as main components with the presence of heptylcyclopentanone and heptylcyclopentane as intermediates. These two compounds were formed at low temperature and further converted to heptadecane and octadecane at high temperature and longer reaction time. A close examination of the reaction over Ni_2P/USY at 4 h reveals that % selective yield of octadecane and heptadecane decreased because these products were cracked to small alkanes. In comparison, CoP/USY showed good performance for both

HDO and DCO/DCO$_2$, pathways according to their almost equal % selective yield, while Ni$_2$P/USY tended to favor the DCO/DCO$_2$ pathway as heptadecane was more abundant than octadecane. Note that the catalytic activity in decarbonylation (DCO) and decarboxylation (DCO$_2$) reactions could not be directly correlated with the amount of CO and CO$_2$ detected in the gas phase because methanation and water gas shift reaction were involved in the main gas-phase reaction. The calculation was therefore based on the liquid products.

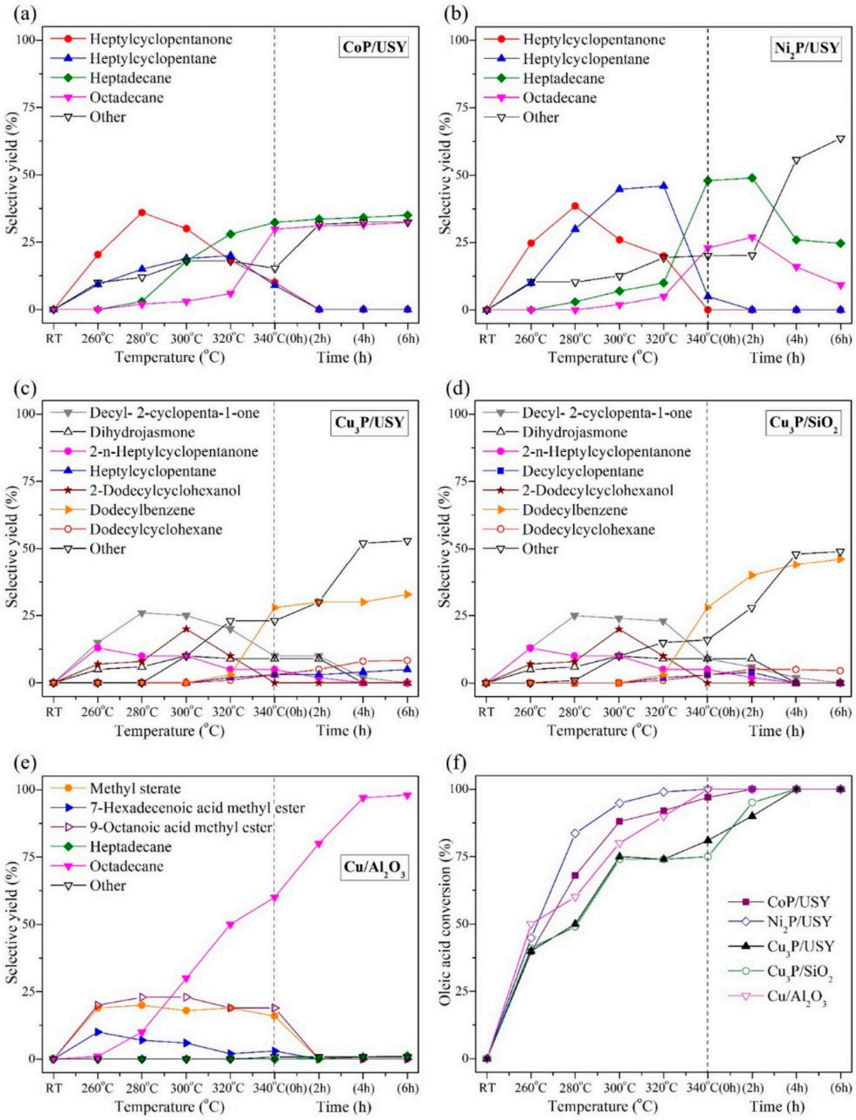

Figure 6. Influence of temperature on deoxygenation of oleic acid over supported metal and metal phosphide catalysts; selectivity (**a**–**e**) and the conversion (**f**).

Cu$_3$P/USY catalyst showed different catalytic behavior. The main product for Cu$_3$P/USY catalyst was dodecylbenzene, and the minor products were identified as dodecylcyclohexane and heptylcyclopentane. Intermediates were cyclic compounds, such as 2-dodecylcyclohexanol and decyl-2-cyclopenta-1-one, being produced at low temperature with oxygen atom and converted to dodecylbenzene at 340 °C. This indicates that several reactions, including HDO, DCO, DCO$_2$, aromatization, and hydrogen transfer, could occur in this reaction system as reported by Tian et al. [34]. The structure of CoP, Ni$_2$P, and Cu$_3$P possesses different Lewis acid sites (metal sites) and Brönsted sites (P–OH sites) that may affect their intrinsic activities. Peroni and coworkers reported that the intrinsic activities of different transition metals have significant impact on the surface reaction of catalysts [35]. However, the support may also have an influence on the activity of catalysts during the reaction. The influence of support materials on the catalytic performance was investigated over supported copper and copper phosphide catalysts (i.e., Cu_3P/USY, Cu_3P/SiO_2, and Cu/γ-Al_2O_3). It was found that Cu_3P/SiO_2 produced similar products as Cu_3P/USY. Interestingly, Cu/γ-Al_2O_3 showed the best selectivity for octadecane production through the HDO pathway (Figure 7) with the highest selective yield (98%), even better than other catalysts. The ester compounds are intermediates which could be observed at lower temperature.

In general reactions, the metal active site favored the alkane products that were obtained from the hydrogenation of oleic acid to octadecanoic acid, and then the water molecule was removed from the octadecanoic acid by dehydration reaction. The Cu/γ-Al_2O_3 could prove that the hydrogen was easier to be adsorbed on metal sites and then added to the oleic acid compound. For Brönsted sites, the heptadecenoic acid was produced from oleic acid by decarboxylation, and then H_2 gas was added into the compound with hydrogenation to provide the heptadecane product. In contrast, for Cu_3P, the oleic acid was transformed to cyclic compounds that have a hexyl ring group or pentyl ring group by cyclization. The water was removed from the compounds by dehydration to form the main product, dodecylbenzene, and then H_2 gas was added into the compounds to produce dodecylcyclohexane and heptylcyclopentane.

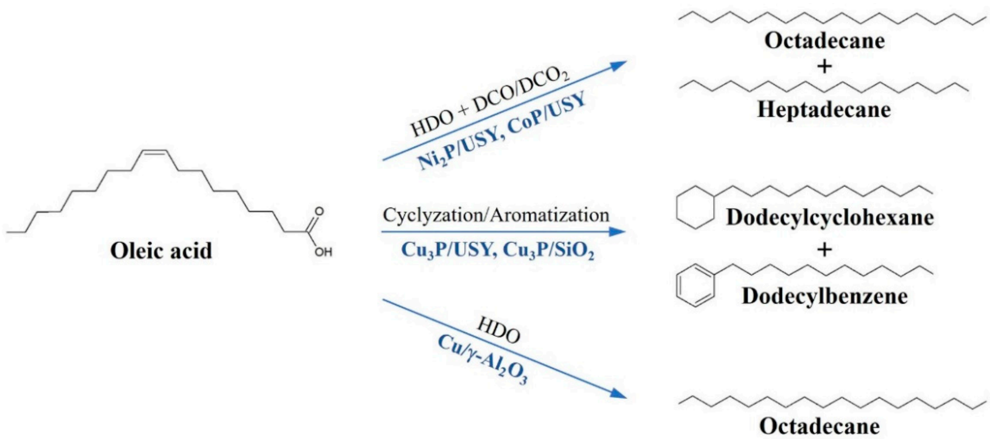

Figure 7. Products obtained from deoxygenation of oleic acid over supported metal and metal phosphides.

3. Materials and Methods

3.1. Materials

$Cu(NO_3)_2{\cdot}3H_2O$ (Univar, 98.0%), $Ni(NO_3)_2{\cdot}6H_2O$ (Univar, 97.0%), $Co(NO_3)_2{\cdot}6H_2O$ (Univar, 98.0%), $(NH_4)_2HPO_4$ (Carlo Erba Reagents, 98.0%), γ-Al_2O_3 (Sasol), SiO_2 (Degussa), and ultrastable zeolite Y (USY) with Si/Al = 13 (Zeolyst International) were used as starting materials.

3.2. Synthesis of Supported Metal Phosphide Catalysts

Copper phosphide catalyst supported on γ-Al_2O_3, SiO_2, and ultrastable zeolite Y (USY) were synthesized by hydrogen reduction of phosphate precursors, according to the previously reported procedure [26,36]. In the first step, the supported copper phosphate precursors were prepared by incipient wetness impregnation method with metal loading of 10 wt%. Copper nitrate and $(NH_4)_2HPO_4$ were dissolved in water with the initial Cu/P molar ratio of 2 and maintained under magnetic stirring. A few drops of nitric acid were added to dissolve some precipitates. Then, SiO_2, γ-Al_2O_3, or USY supports were added into the solution under continuous stirring for 30 min, followed by ultrasonication for 3 h. The obtained phosphate precursor mixture was dried at 80 °C for 12 h and calcined in air at 450 °C for 3 h. In the second step, the metal phosphate precursors were reduced to phosphide catalysts in hydrogen atmosphere with a ramp rate of 5 °C/min from room temperature to 650 °C and kept at isothermal conditions for 5 h.

Other supported metal phosphides (i.e., Ni_2P/USY, CoP/USY) were prepared from the corresponding metal nitrates, with the same metal loading and metal/P molar ratio, using the described procedure. As the reduction of cobalt phosphate has been reported to occur at higher temperature (~700–720 °C) than that of nickel phosphate (~600–650 °C) [37,38], the hydrogen reduction temperatures of Ni_2P/USY and CoP/USY were 650 °C and 750 °C, respectively.

3.3. Characterization of Supported Metal Phosphide Catalysts

X-ray diffraction (XRD) patterns were measured on a powder diffractometer (D8 ADVANCE, Bruker, Karlsruhe, Germany) using Cu Kα radiation with Ni filter, operated at 40 kV and 40 mA, in the 2θ range of 10–80°. The average crystallite size of catalysts, *D*, was calculated using the Debye–Scherrer formula and FullProf software [39] as described below.

$$D = K\lambda/\beta\cos\theta \tag{1}$$

where λ is the X-ray wavelength (nm), β is the integral breadth of diffraction peak, and *K* is a constant related to crystallite shape. LaB_6 was used as a standard to determine the instrumental resolution of the X-ray diffractometer. The scanning electron microscopy (SEM) analysis was performed using a HITACHI SU5000 FE-SEM microscope operating at 10 kV in back-scattering electron (BSE) mode. Nitrogen adsorption–desorption isotherms were recorded at −196 °C using a Nova 2000e analyzer (Quantachrome Instruments) after each sample was degassed at 300 °C for 3 h. The surface area and the pore-size distribution of catalysts were determined by using the Brunauer–Emmett–Teller (BET) and Barrett–Joyner–Halenda (BJH) methods, respectively. T-plot analysis was additionally applied to evaluate the surface area and volume of micropores. Temperature-programmed desorption (TPD) of NH_3 analysis was conducted using an automated ChemBET Pulsar TPR/TPD chemisorption analyzer (Quantachrome instruments). Catalyst (100 mg) was loaded and pretreated in He at 120 °C for 1 h. Afterward, NH_3-TPD was performed in flowing H_2/Ar gas mixture (H_2/Ar = 1.5; total flow 30 cm^3 min^{-1}) and heated to 800 °C at a heating rate of 5 °C/min.

3.4. Deoxygenation of Oxygenated Hydrocarbon Compounds

Deoxygenation reaction of the oxygenated model compound, oleic acid, was carried out in a Parr reactor. A 1 g portion of supported metal phosphide catalyst and 60 mL of 5 wt% solution of oleic acid in dodecane were loaded into the reactor. Prior to the reaction, the reactor was purged with N_2, then heated to 240 °C and pressurized with H_2 to 50 bar. The catalytic activities were measured at 260 °C, 280 °C, 300 °C, 320 °C, 340 °C, and at two-hour intervals for six hours at 340 °C. All obtained products were analyzed by a gas chromatograph–mass spectrometer (GC-MS) with a DB-1HT capillary column. Note that the gas-phase products in this study, such as C_4H_{10}, C_3H_8, C_2H_6, CH_4, CO, and CO_2, were not analyzed because methanation and water gas shift reaction were involved in the main gas-phase reaction. The calculation was therefore based on the liquid products. All standard calibration curves of C_{13}-C_{18} were used for quantitative analysis. Moreover, 8 mg of C_{15} was added into the sample as an internal standard for Cu_3P/SiO_2 and Cu_3P/USY catalysts. The conversion of oleic acid was calculated according to the following equations:

$$\text{conversion}(\%) = \frac{\text{mole of oleic acid in feed} - \text{mole of oleic acid in product}}{\text{mole of oleic acid in feed}} \times 100 \tag{2}$$

The selective yield (*Y*) of products was calculated based on carbon mass balance [3]:

$$Y_i(\text{mol\%}) = \left(\frac{n_i \times a_i}{n_{Oleic\ acid} \times a_{Oleic\ acid}}\right) \times 100 \tag{3}$$

where n_i and a_i represent the mole and carbon atom number of product i. $n_{Oleic\ acid}$ and $a_{Oleic\ acid}$ represent the mole of oleic acid and carbon atom number of oleic acid, respectively. The quantitative analyses were mostly conducted on HDO and DCO/DCO_2 products. The unspecified liquid products could refer to the cyclic or aromatic compounds and polymerized products.

4. Conclusions

Supported copper, nickel, and cobalt phosphide catalysts were evaluated for deoxygenation of oleic acid. The oleic acid was chosen as a model compound with the aim to gain insight into the deoxygenation reaction of fatty acids, a key step in the conversion of renewable biofuel to fuels and value-added chemicals. We have demonstrated that different catalysts exhibited different catalytic behaviors. The nature of the support materials has a profound effect on the structural, surface, and catalytic properties of Cu_3P. All supported metal phosphides were prepared by the hydrogen reduction of impregnated metal phosphate precursors. CoP and Ni_2P were formed on USY zeolite. Cu_3P was formed on USY and SiO_2 supports, while the metallic Cu phase was stabilized on γ-Al_2O_3 support. Metal phosphide particles were highly dispersed over the surface of the USY support. Cu_3P/USY exhibited much larger surface area and higher concentration of acid sites compared to Cu_3P/SiO_2, owing to the textural and acidic properties of the USY zeolite support. All supported catalysts gave an oleic acid conversion close to 100% at 340 °C. The main hydrocarbon products of Ni_2P/USY and CoP/USY were heptadecane and octadecane derived from DCO/DCO_2 and HDO pathways, respectively. Cu/γ-Al_2O_3 facilitated the HDO reaction and inhibited cracking reactions, leading to the highest selective production of octadecane (98%). In contrast, the supported Cu_3P catalysts favored cyclization and aromatization to form cyclic and aromatic compounds such as dodecylcyclohexane, heptylcyclopentane, and dodecylbenzene. Cu_3P/SiO_2 gave higher selective yield of dodecylbenzene (46%) than the Cu_3P/USY (33%). Therefore, we may conclude that the supported Cu_3P catalysts have potential applications in the production of cyclic and aromatic compounds, while Cu/γ-Al_2O_3 can be considered as a promising catalyst for the hydrodeoxygenation of renewable biofuel to alkane products. We believe that this study can provide new ideas and directions for the development of renewable biofuel energy in the future.

Author Contributions: Conceptualization, C.K. and P.K.; data curation, N.K., C.K., and P.K.; investigation, N.K., T.B., and S.K.; methodology, C.K. and P.K.; project administration, C.K. and P.K.; supervision, C.K., P.K., A.W., and K.F.; writing—original draft preparation, N.K., C.K., and P.K.; writing—review and editing, N.K., C.K., P.K., T.B., S.K., A.W., and K.F.

Funding: This research was co-supported by the Graduate Program Scholarship from the Graduate School, Kasetsart University, Kasetsart University Research and Development Institute (KURDI), Thailand Research Fund (TRG5780192) and National Nanotechnology Center (NANOTEC), NSTDA, Ministry of Science and Technology, Thailand, through its program of Research Network NANOTEC (RNN).

Conflicts of Interest: The authors declare no conflict of interest.

References

1. Meier, D.; van de Beld, B.; Bridgwater, A.V.; Elliott, D.C.; Oasmaa, A.; Preto, F. State-of-the-art of fast pyrolysis in IEA bioenergy member countries. *Renew. Sustain. Energy Rev.* **2013**, *20*, 619–641. [CrossRef]
2. Furimsky, E. Hydroprocessing challenges in biofuels production. *Catal. Today* **2013**, *217*, 13–56. [CrossRef]
3. Zuo, H.; Liu, Q.; Wang, T.; Ma, L.; Zhang, Q.; Zhang, Q. Hydrodeoxygenation of Methyl Palmitate over Supported Ni Catalysts for Diesel-like Fuel Production. *Energy Fuels* **2012**, *26*, 3747–3755. [CrossRef]
4. Arun, N.; Sharma, R.V.; Dalai, A.K. Green diesel synthesis by hydrodeoxygenation of bio-based feedstocks: Strategies for catalyst design and development. *Renew. Sustain. Energy Rev.* **2015**, *48*, 240–255. [CrossRef]
5. Cheng, S.; Wei, L.; Zhao, X.; Julson, J. Application, Deactivation, and Regeneration of Heterogeneous Catalysts in Bio-Oil Upgrading. *Catalysts* **2016**, *6*, 195. [CrossRef]
6. Si, Z.; Zhang, X.; Wang, C.; Ma, L.; Dong, R. An Overview on Catalytic Hydrodeoxygenation of Pyrolysis Oil and Its Model Compounds. *Catalysts* **2017**, *7*, 169. [CrossRef]

7. Mortensen, P.M.; Grunwaldt, J.D.; Jensen, P.A.; Knudsen, K.G.; Jensen, A.D. A review of catalytic upgrading of bio-oil to engine fuels. *Appl. Catal. A* **2011**, *407*, 1–19. [CrossRef]
8. Wang, Y.; He, T.; Liu, K.; Wu, J.; Fang, Y. From biomass to advanced bio-fuel by catalytic pyrolysis/hydro-processing: Hydrodeoxygenation of bio-oil derived from biomass catalytic pyrolysis. *Bioresour. Technol.* **2012**, *108*, 280–284. [CrossRef]
9. Kim, T.S.; Oh, S.Y.; Kim, J.Y.; Choi, I.G.; Choi, J.W. Study on the hydrodeoxygenative upgrading of crude bio-oil produced from woody biomass by fast pyrolysis. *Energy* **2014**, *68*, 437–443. [CrossRef]
10. Yao, G.; Wu, G.; Dai, W.; Guan, N.; Li, L. Hydrodeoxygenation of lignin-derived phenolic compounds over bi-functional Ru/H-Beta under mild conditions. *Fuel* **2015**, *150*, 175–183. [CrossRef]
11. Lee, H.W.; Jun, B.R.; Kim, H.; Kim, D.H.; Jeon, J.K.; Park, S.H.; Ko, C.H.; Kim, T.W.; Park, Y.K. Catalytic hydrodeoxygenation of 2-methoxy phenol and dibenzofuran over Pt/mesoporous zeolites. *Energy* **2015**, *81*, 33–40. [CrossRef]
12. Itthibenchapong, V.; Ratanatawanate, C.; Oura, M.; Faungnawakij, K. A facile and low-cost synthesis of MoS_2 for hydrodeoxygenation of phenol. *Catal. Commun.* **2015**, *68*, 31–35. [CrossRef]
13. Leiva, K.; Sepulveda, C.; García, R.; Laurenti, D.; Vrinat, M.; Geantet, C.; Escalona, N. Kinetic study of the conversion of 2-methoxyphenol over supported Re catalysts: Sulfide and oxide state. *Appl. Catal. A* **2015**, *505*, 302–308. [CrossRef]
14. Wang, W.; Yang, Y.; Luo, H.; Liu, W. Effect of additive (Co, La) for Ni–Mo–B amorphous catalyst and its hydrodeoxygenation properties. *Catal. Commun.* **2010**, *11*, 803–807. [CrossRef]
15. Wang, W.; Yang, S.; Qiao, Z.; Liu, P.; Wu, K.; Yang, Y. Preparation of Ni–W–P–B amorphous catalyst for the hydrodeoxygenation of *p*-cresol. *Catal. Commun.* **2015**, *60*, 50–54. [CrossRef]
16. Santillan-Jimenez, E.; Perdu, M.; Pace, R.; Morgan, T.; Crocker, M. Activated Carbon, Carbon Nanofiber and Carbon Nanotube Supported Molybdenum Carbide Catalysts for the Hydrodeoxygenation of Guaiacol. *Catalysts* **2015**, *5*, 424–441. [CrossRef]
17. Monnier, J.; Sulimma, H.; Dalai, A.; Caravaggio, G. Hydrodeoxygenation of oleic acid and canola oil over alumina-supported metal nitrides. *Appl. Catal. A* **2010**, *382*, 176–180. [CrossRef]
18. Afanasiev, P.; Laurenti, D. CCl4-Assisted Preparation of Highly Dispersed Molybdenum and Tungsten Nitrides. *Top. Catal.* **2012**, *55*, 940–949. [CrossRef]
19. Prins, R.; Bussell, M.E. Metal phosphides: Preparation, characterization and catalytic reactivity. *Catal. Lett.* **2012**, *142*, 1413–1436. [CrossRef]
20. Consuelo Alvarez-Galvan, M.; Campos-Martin, J.M.; Fierro, J.L.G. Transition Metal Phosphides for the Catalytic Hydrodeoxygenation of Waste Oils into Green Diesel. *Catalysts* **2019**, *9*, 293. [CrossRef]
21. Iino, A.; Cho, A.; Takagaki, A.; Kikuchi, R.; Oyama, S.T. Kinetic studies of hydrodeoxygenation of 2-methyltetrahydrofuran on a Ni_2P/SiO_2 catalyst at medium pressure. *J. Catal.* **2014**, *311*, 17–27. [CrossRef]
22. Moon, J.S.; Kim, E.G.; Lee, Y.K. Active sites of Ni_2P/SiO_2 catalyst for hydrodeoxygenation of guaiacol: A joint XAFS and DFT study. *J. Catal.* **2014**, *311*, 144–152. [CrossRef]
23. Cecilia, J.A.; Infantes-Molina, A.; Rodríguez-Castellón, E.; Jiménez-López, A.; Oyama, S.T. Oxygen-removal of dibenzofuran as a model compound in biomass derived bio-oil on nickel phosphide catalysts: Role of phosphorus. *Appl. Catal. B* **2013**, *136*, 140–149. [CrossRef]
24. Zhao, H.Y.; Li, D.; Bui, P.; Oyama, S.T. Hydrodeoxygenation of guaiacol as model compound for pyrolysis oil on transition metal phosphide hydroprocessing catalysts. *Appl. Catal. A* **2011**, *391*, 305–310. [CrossRef]
25. Zhang, X.; Wang, T.; Ma, L.; Zhang, Q.; Yu, Y.; Liu, Q. Characterization and catalytic properties of Ni and NiCu catalysts supported on ZrO_2–SiO_2 for guaiacol hydrodeoxygenation. *Catal. Commun.* **2013**, *33*, 15–19. [CrossRef]
26. Soták, T.; Schmidt, T.; Hronec, M. Hydrogenolysis of polyalcohols in the presence of metal phosphide catalysts. *Appl. Catal. A* **2013**, *459*, 26–33. [CrossRef]
27. Shi, H.; Chen, J.; Yang, Y.; Tian, S. Catalytic deoxygenation of methyl laurate as a model compound to hydrocarbons on nickel phosphide catalysts: Remarkable support effect. *Fuel Process. Technol.* **2014**, *118*, 161–170. [CrossRef]
28. Burns, A.W.; Layman, K.A.; Bale, D.H.; Bussel, M.E. Understanding the relationship between composition and hydrodesulfurization properties for cobalt phosphide catalysts. *Appl. Catal. A* **2008**, *343*, 68–76. [CrossRef]
29. Weidenthaler, C.; Schmidt, W. Thermal Stability and Thermal Transformations of Co^{2+}- or Ni^{2+}-Exchanged Zeolites A, X, and Y. *Chem. Mater.* **2000**, *12*, 3811–3820. [CrossRef]

30. Möller, K.; Bein, T. Mesoporosity—A new dimension for zeolites. *Chem. Soc. Rev.* **2013**, *42*, 3689–3707. [CrossRef]
31. Huang, C.; Lia, A.; Chao, Z.S. Heterogeneous catalytic synthesis of quinoline compounds from aniline and C_1–C_4 alcohols over zeolite-based catalysts. *RSC Adv.* **2017**, *7*, 48275–48285. [CrossRef]
32. Li, K.; Wang, R.; Chen, J. Hydrodeoxygenation of Anisole over Silica-Supported Ni_2P, MoP, and NiMoP Catalysts. *Energy Fuels* **2011**, *25*, 854–863. [CrossRef]
33. Gafurov, M.R.; Mukhambetov, I.N.; Yavkin, B.V.; Mamin, G.V.; Lamberov, A.A.; Orlinskii, S.B. Quantitative Analysis of Lewis Acid Centers of γ-Alumina by Using EPR of the Adsorbed Anthraquinone as a Probe Molecule: Comparison with the Pyridine, Carbon Monoxide IR, and TPD of Ammonia. *J. Phys. Chem. C* **2015**, *119*, 27410–27415. [CrossRef]
34. Tian, Q.; Qiao, K.; Zhou, F.; Chen, K.; Wang, T.; Fu, J.; Lu, X.; Ouyang, P. Direct Production of Aviation Fuel Range Hydrocarbons and Aromatics from Oleic Acid without an Added Hydrogen Donor. *Energy Fuels* **2016**, *30*, 7291–7297. [CrossRef]
35. Peroni, M.; Lee, I.; Huang, X.; Baráth, E.; Gutierrez, O.Y.; Lercher, J.A. Deoxygenation of Palmitic Acid on Unsupported Transition-Metal Phosphides. *ACS Catal.* **2017**, *7*, 6331–6341. [CrossRef]
36. Oyama, S.T.; Wang, X.; Lee, Y.K.; Bando, K.; Requejo, F.G. Effect of phosphorus content in nickel phosphide catalysts studied by XAFS and other techniques. *J. Catal.* **2002**, *210*, 207–217. [CrossRef]
37. Bui, P.; Cecilia, J.A.; Oyama, S.T.; Takagaki, A.; Infantes-Molina, A.; Zhao, H.; Li, D.; Rodríguez-Castellón, E.; López, A.J. Studies of the synthesis of transition metal phosphides and their activity in the hydrodeoxygenation of a biofuel model compound. *J. Catal.* **2012**, *294*, 184–198. [CrossRef]
38. Wang, X.; Clark, P.; Oyama, S.T. Synthesis, Characterization, and Hydrotreating Activity of Several Iron Group Transition Metal Phosphides. *J. Catal.* **2002**, *208*, 321–331. [CrossRef]
39. Rodríguez-Carvajal, J. Recent Developments of the Program FULLPROF. In *Newsletter*; Commission on Powder Diffraction (IUCr): Chester, UK, 2001; Volume 26, pp. 12–19.